Shape from Shading Using Multiple Detector Signals in Scanning Electron Microscopy

L. Reimer
Universität Münster

R. Böngeler
Universität Münster

V. Desai
Universität Münster

Recommended Citation

Utah State University
MERRILL-CAZIER LIBRARY

SHAPE FROM SHADING USING MULTIPLE DETECTOR SIGNALS IN SCANNING ELECTRON MICROSCOPY

L. Reimer*, R. Böngeler, V. Desai

Physikalisches Institut, Universität Münster
Wilhelm-Klemm-Straße 10, D-4400 Münster, FRG

Abstract

Using a two- or multiple detector system for secondary electrons (SE) or backscattered electrons (BSE) the difference signal can be used to reconstruct the surface profile. Micrographs recorded by these difference signals are more like shaded images obtained by illumination from one side than conventional micrographs using only one detector. Therefore, the concept of the shape-from-shading method developed for light illumination can be transferred to scanning electron microscopy as long as one considers the characteristic differences in signal detection and image formation. The surface tilt contrast causes signal differences A-B when using a two-detector system of opposite Everhart-Thornley or semiconductor detectors which are linearly to the surface gradient $\partial z/\partial x$ for SE and proportional to $\sin \Phi \cos \chi$ for BSE in first order approximation, where Φ denotes the surface tilt angle relative to the electron beam and χ an azimuth. This allows us to reconstruct the surface profile by analogue or digital image processing.

Plots of isodensities from a spherical specimen or in a gradient plane correspond to a parallel and gnomonic projection of a sphere, respectively, and are useful to compare different detector systems. The signals of SE and BSE can be self-shadowed by the specimen. The influence of the shadowing on the surface reconstruction can be reduced by an iterative correction method.

*Address for correspondence:
 L. Reimer, Physikalisches Institut
 Universitat Muenster, Wilhelm-Klemm-Strasse 10
 D-4400 Muenster, FRG.
                        Phone no.: (0251) 83 36 22

Introduction

The dependence of light reflectance on local surface tilt can be used for a reconstruction of the surface by calculating the shape from the shading (Horn 1977, Ikeuchi and Horn 1981, Horn and Brooks 1986). Multiple images illuminated from different directions contain additional information about the azimuthal orientation of a surface facet (Woodham 1981). This leads to a method called photometric stereo. Both of these methods of stereophotometry also allow us to reconstruct the shape of uniform surfaces, whereas the traditional stereometry needs the measurement of a parallax between corresponding sharply defined points in two images. In the future, a digital image processing system should combine both methods. Also, shape from shading is not only of interest for the reconstruction of surface topography but can also be used for a better separation of particles in stereology and statistical applications of image processing.

Because of the similarity between images recorded by light illumination and by a scanning electron microscope (SEM), these methods can be transferred to SEM micrographs as shown by Ikeuchi and Horn (1981). We describe in this paper the difference between light and SEM micrographs due to the theorem of reciprocity and develop a refinement of this shape-from-shading method by taking into account the electron-specimen interactions and the different mechanisms of signal formation. Information about the surface shape can be better realised by using multiple detector systems for secondary (SE) and backscattered electrons (BSE) which correspond to illuminations from different directions in light optics. The image intensity not only depends on the surface tilt but also on material. Shadowing effects have to be taken into account and the diffusion of primary electrons results in an enhanced image intensity at edges, for example, which has no counterpart in light illumination. Backscattered electrons can strike other surface elements which also results in enhanced image intensity and is analogous to mutual illumination by light when a valley is illuminated by a mountain at sunset, for example. Measurements and calculations of the BSE signals for edges and surface steps have been reported by Reimer et al. (1986) and Reimer and Stelter (1987).

List of Symbols

E	=	Electron energy
p,q	=	Coordinates of the gradient plane
R	=	Electron range
S	=	Detector signal
t	=	Exit depth of secondary electrons
u,v	=	Projected plane coordinates of a sphere
x	=	Coordinate parallel linescans
z	=	Coordinate antiparallel to the electron beam
Z	=	Atomic number
ß	=	Mean number of SE per BSE / mean number of SE excited by the primary electrons at normal incidence
δ	=	Secondary electron yield
ζ	=	Take-off angle between detector D and surface normal N
η	=	Backscattering coefficient
ξ	=	Take-off angle between detector D and electron beam P
Φ	=	Surface tilt angle between the primary beam P and the surface normal N
σ	=	Prefactor of detector signals dependent on surface tilt
χ	=	azimuth angle
ψ	=	take-off angle of shadowing

Therefore, common computation methods for light and SEM images will be of interest and experiences in both fields can compliment each other. An image processing routine containing a-priori knowledge about the physics of electron emission and image information will allow us the interpretation of SEM micrographs. The analogy of image contrast caused by light and electron emission is an advantage of SEM but the differences can result in misinterpretation by an untrained user.

Dependence of SE and BSE emission on surface tilt and material

The total backscattering coefficient η is defined as the fraction of primary electrons (PE) that leaves the specimen by multiple elastic large-angle scattering and electron diffusion (see Niedrig 1982, Reimer 1985, Wells 1974 for reviews). This coefficient increases monotonously with increasing atomic number Z and surface tilt angle Φ between surface normal and electron incidence (Fig.1) and measurements of η can be fitted by a formula proposed by Darlington (1975) for electron energy E = 20 keV:

$$\eta(Z,\Phi) = B\ (n_0/B)^{\cos \Phi} \quad \text{with B = 0.89 and} \quad (1)$$

$$n_0 = -0.0254+0.016\ Z-1.86\times10^{-4}Z^2+8.3\times10^{-7}Z^3$$

for example, where n_0 denotes the backscattering coefficient for normal incidence (Φ=0). For a multi-component target the mixing rule (Castaing 1960, Herrmann and Reimer 1984):

$$\eta = \sum_{i=1}^{n} c_i\ \eta_i \qquad (2)$$

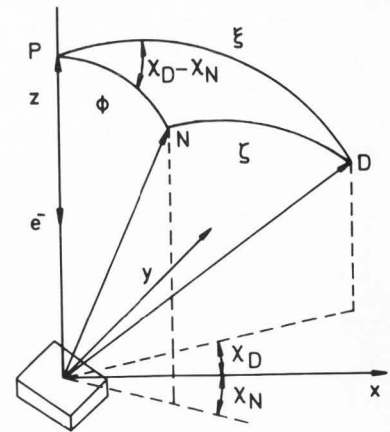can be used where c_i are the mass fractions of the

Fig.1. Angles for characterizing the primary electron beam P (viewer), surface normal N and the take-off direction D of the detector (light source) in scanning electron microscopy and in (light optics), respectively.

elements and the n_i are the backscattering coefficients of the pure elements. In the range E = 5-100 keV, the backscattering coefficient is approximately independent on electron energy E. For E < 5 keV see measurements by Reimer and Tollkamp (1980) and Monte Carlo calculations by Lödding and Reimer (1981) and Reimer and Stelter (1986).

The angular distribution of the BSE approximately follows Lambert's law:

$$\frac{dn}{d\Omega} = \frac{n}{\pi} \cos \zeta \qquad (3)$$

for normal incidence (Φ=0) where ζ is the angle between surface normal and take-off direction (Kanter 1957, Drescher et al. 1970). The fraction of BSE backscattered opposite to the electron beam with angles ξ < π/2 also follows such a law up to tilt angles Φ < 50°-60° whereas the increase of η with increasing Φ described by Eq. (1) is concentrated in a reflection-like maximum that becomes more pronounced with increasing Φ. For a more detailed discussion, it is necessary to look on the dependence of dη/dΩ on the take-off angle ξ and the azimuthal angle x_D of the detector. The result is a broad distribution of dn/dΩ in dependence on x_D (Reimer and Riepenhausen 1984, 1985). This means that the often used phrase "reflection-like" or specular reflection will not be a good description for the shape of dη/dΩ.

The energy distribution of BSE consists of a most probable energy of the order of 0.9 E for high and 0.6 E for low Z material where E = eU is the primary electron energy. The signal intensity of BSE detectors depends on the energy of the BSE (see below). The BSE move on straight trajectories between specimen and detector. The knowledge of $d^2n/dEd\Omega$ will be necessary for a correct discussion of signal intensity though no experimental results and calculations exist about this function. Therefore, the dependence of the signal intensity on the tilt angle Φ and on azimuthal angle x_N of the surface normal has to be recorded experimentally for a given type of detector and

geometry. This can be realised by scanning a sphere that contains all tilt and azimuthal angles (Lange et al. 1984) or by scanning a cone with a fixed angle Φ and varying x_N.

Secondary electrons are generated by inelastic excitations. Their most probable energy is of the order of 2-5 eV and they can leave the specimen only from a thin surface layer t of the order of a few nanometres. The secondary electron yield δ consists of a contribution δ_{PE} excited by the primary electrons (PE) that is proportional to $t_0 t_8$ sec Φ as the path length within t and to $E^{-0.8}$ as an approximation of the Bethe stopping power proportional to $dE/ds \propto (1/E) \ln (E/J)$ in the range E = 5-30 keV (J = mean ionisation energy). A second contribution δ_{BSE} is excited by the BSE on their trajectories through the surface layer and a factor β of the order of 2-3 (Drescher et al. 1970, Reimer and Drescher 1977) considers the mean increase of secondary electron emission per BSE caused by the lowered exit energy and the increase of path lengths due to the angular distribution:

$$\delta = \delta_{PE} + \delta_{BSE} = \delta_0 (\sec \Phi + \beta\eta) \simeq \delta(0) \sec^n \Phi \quad (4)$$

with $0.65 < n < 1.3$. This superposition of SE generation by PE and BSE results in an experimental dependence of δ on Φ that can be approximated by a $\sec^n \Phi$ law where $\delta(0)$ is the total SE yield at $\Phi=0$ as shown in Fig.2 in a double-logarithmic plot for a primary electron energy of 9.3 keV. The exponent n as the slope of the straight lines decreases from $n \simeq 1.3$ for Be to $n \simeq 1.1$ for Al and $n \simeq 0.65$ for Au. This exponent is independent on primary electron energy E in the range 10-100 keV, only $\delta(0)$ decreases proportional to $E^{-0.8}$ with increasing E. The increase of the second term in Eq.(4) with increasing η or Z results in an increase of $\delta(0)$ though the influence of surface layers on δ results in a larger scatter of experimental values (Drescher et al. 1970).

Though exact measurements of the angular exit distribution $d\delta/d\Omega$ of SE become difficult due to the low exit energy of SE, all experiments and theoretical approaches confirm that a Lambert law can be used for the emission of SE:

$$\frac{d\delta}{d\Omega} = \frac{\delta(\Phi)}{\pi} \cos \zeta = \frac{1}{\pi} \delta(0) \sec^n \Phi \cos \zeta \quad (5)$$

Detection of SE and BSE in SEM

The widely used Everhart-Thornley detector (ETD) for SE consists of a collector grid positively biased at a few hundred volts to attract the low-energy SE (Everhart and Thornley 1960). Behind the grid, a scintillator biased at +10 kV accelerates the SE so that they produce a large number of photons in the scintillator which can be recorded through a light-pipe by a photomultiplier tube. Such a detector shows optimum detection quantum efficiency (DQE) and a large bandwidth from zero to megahertz frequencies. However, this detector does not collect all emitted SE; those with exit momenta opposite to the detector can fly on trajectories which end on the final
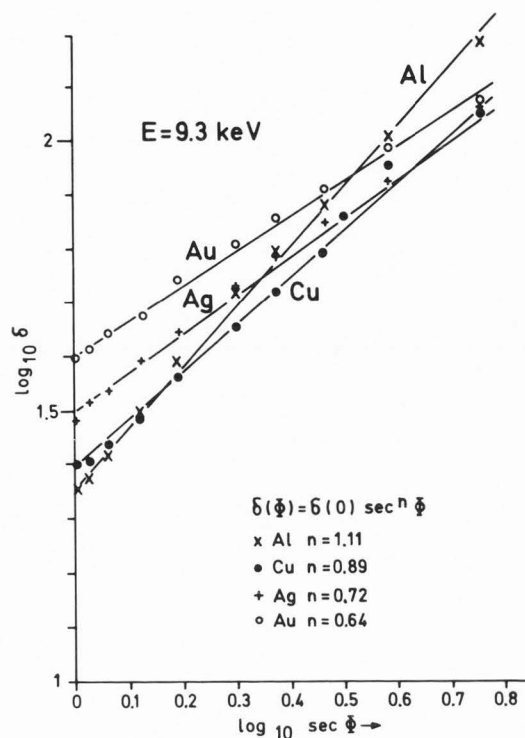

Fig.2. Double-logarithmic plot of the secondary electron yield δ versus sec Φ for demonstrating the validity of $\delta \propto \sec^n \Phi$.

polepiece plate above the specimen. The fraction of collected SE depends on the size and geometry of the specimen and on the working distance that is the distance between specimen and polepiece plate.

There are three possible detection systems for backscattered electrons:
1. A scintillator-photomultiplier combination as used in the Everhart-Thornley detector for SE. Because the BSE trajectories are not affected by electrostatic collection fields, the scintillator has to be mounted with a large solid angle of collection at different take-off direction depending on the wanted contrast information.
2. A semiconductor detector of the surface-barrier type. A few thousands of electron-hole pairs are generated per BSE and can be separated in the depletion layer of a p-n junction. Contrary to a scintillator-photomultiplier combination, this detector shows a reduced bandwidth of the order of a few hundreds of kilohertz. When a semiconductor detector shall be used at higher frequencies, the electron-probe current and the solid angle of collection have to be increased.
3. A BSE-to-SE converter plate (Fig.3) below the polepiece, for example (Moll et al. 1979, Reimer and Volbert 1979, 1980a). SE are generated by the BSE at a MgO coated plate behind an earthed grid. The SE can be collected by the Everhart-Thornley detector. A positive bias U_C of the converter plate retards the excited SE

(Fig.3a) and a negatively biased plate accelerates the SE (Fig.3b) so that they can pass the earthed grid and are collected by the ETD. This allows us to switch on and off the BSE detection and to use the ETD for the detection of both SE and BSE sequentially.

Detection of BSE by scintillator or semiconductor detectors results in a preferential contribution of high-energy BSE proportional to $E_{BSE}-E_{th}$ where $E_{th} \simeq 1$ keV is a threshold energy. For $E < 20$-30 keV, the signal of a BSE-to-SE converter coated with MgO is independent of the energy of the BSE due to charging effects. Using a metal plate as a converter, the BSE signal becomes proportional to $E_{BSE}^{0.8}$ and low-energy BSE preferentially contribute to the signal.
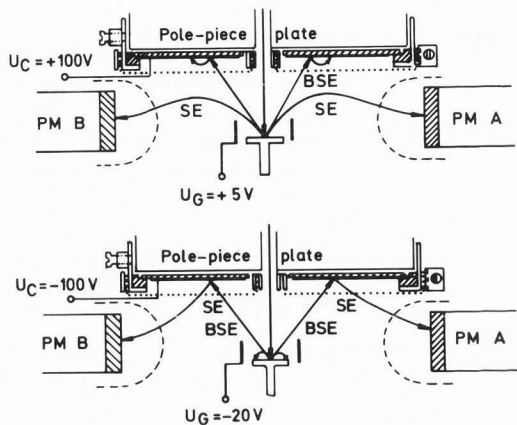

Fig.3. Two-detector system consisting of opposite Everhart-Thornley detectors and a BSE-to-SE converter plate below the polepiece plate and a ring electrode around the specimen. The system can be switched from the a) SE to the b) BSE mode by changing the biases of the ring and the converter plate.

Multiple detector systems

At first, Kimoto et al. (1966) proposed two semi-annular semiconductor detectors below the polepiece and demonstrated that their sum signal shows predominantly material contrast and suppressed topographic contrast whereas the difference signal shows topographic and suppressed material contrast. However, a wrong apparent topographic contrast results at interfaces of low and high mean atomic numbers due to an anisotropic electron diffusion (Reimer and Volbert 1980b, 1982; Reimer 1982, 1984). Lebiedzik (1979), Lebiedzik and White (1975), Lebiedzik et al. (1979) used four semiconductor detectors at $\xi = 45°$. A similar system using four scintillators is proposed by Jackman (1980).

We proposed a two-detector system for SE and BSE shown in Fig.3 (Volbert and Reimer 1980, Reimer 1982). A ring electrode around the specimen screens the collector grids of the opposite ETDs so that the SE can fly on straight trajectories before entering the collection fields of detectors A and B depending on their exit momenta

(Fig.3a). A negative bias U_G of the ring electrode retards the SE and the negatively biased BSE-to-SE converter plate below the polepiece allows us to record the converted SE by the detectors A and B (Fig.3b).

Another SE multiple detector system consists of two opposite Everhart-Thornley detectors which can be turned from a connection axis parallel x to a position with an axis parallel to y (Reimer and Riepenhausen 1985).

We assume that the detectors A and B of a two-detector system collect all SE and BSE emitted to the right-hand and left-hand side, respectively. This means that the detectors A and B record sectors of a Lambert's distribution differently shaded in Fig.4. Integration of this distribution $\propto \cos \Phi$ from a plane surface ($\psi_{A,B}=0$) over the solid angle results in a signal (Reimer 1982, Lange et al. 1984):
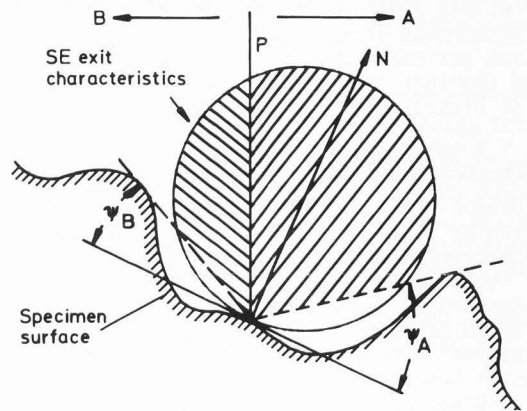

Fig.4. Fraction of collected SE from the Lambertian exit characteristics by detectors A and B and consideration of self-shadowing of the specimen.

$$S_{A,B} \propto \sigma(\Phi) \frac{1}{2} (1 \pm \sin \Phi \cos \chi_N) \qquad (6)$$

with the positive and negative signs for the detectors A and B, respectively, where $\sigma(\Phi)$ denotes the total collected fraction of either the secondaries or backscattered electrons. The non-zero angles $\psi_{A,B}$ in Fig.4 consider the self-shadowing by the surface topography. For a surface profile $z(x)$ independent on y (surface steps on IC and scratches by grinding, for example), the azimuthal angle χ_N becomes zero and the shadowing can be considered by modifying Eq.(6):

$$S_{A,B} \propto \sigma(\Phi) \frac{1}{2} (\cos \psi_{A,B} \pm \sin \Phi) \qquad (7)$$

For the secondaries, we make use of $\sigma(\Phi)=\delta(0) \sec^n \Phi$ (equation 4). For the backscattered electrons, we assume that $\sigma(\Phi) = \eta_0$ is approximately independent on Φ for $0<\Phi< 60°$ because a BSE detector system normally only collects BSE with $\xi<90°$ and because the increase of η with increasing η is mainly concentrated in directions $\xi>90°$. This can be described by a decrease of the total BSE signal proportional to $\cos^m \Phi$, where $0<m<0.5$, though this will only be a rough approximation because a more accurate description needs the consideration of $d\eta/d\Omega$. For semi-annular BSE

detectors with $0 < \xi < 90°$, for example, $\sigma(\Phi)$ can even increase with increasing Φ before passing a maximum (Reimer and Riepenhausen 1985). Both cases, we combine in:

$$\sigma(\Phi) \propto \cos^k \Phi \qquad (8)$$

with $-1.3 < k < -0.65$ and $0 < k < 0.5$ for SE and BSE, respectively.

When setting $\psi_{A,B} = 0$ for simplicity, the difference and sum signals of Eq. (6) become:

$$S_A - S_B \propto \sigma(\Phi) \sin \Phi \cos x_N \qquad (9a)$$
$$S_A + S_B \propto \sigma(\Phi) \qquad (9b)$$

where the difference signal Eq. (9a) contains azimuthal information of the surface normal in the last cosine term, whereas the sum signal Eq. (9b) only contains information about material and the absolute value of the surface tilt Φ. Equation (9a) can be confirmed by recording isodensities of SE and BSE signals (Figs.5a-d) using a steel ball as a test specimen that contains all tilt and azimuthal angles at coordinates

$$u = \sin \Phi \cos x_N \quad \text{and} \quad v = \sin \Phi \sin x_N \qquad (10)$$

with the origin at the image centre of the sphere (Lange et al. 1984). Figures 6a-d show the calculated isodensities using $\sigma(\Phi) \propto \sec \Phi$ and $\sigma(\Phi) \propto \cos^{\frac{1}{2}} \Phi$ for SE and BSE, respectively. The correspondence of the measured and calculated isodensities in Figs. 5 and 6 confirm these approximations for the SE and BSE signals. Straight parallel and equidistant isodensities which can be observed at the central part of the sphere ($\Phi < 60°$) in Figs.5d and 6d are a test that the BSE A-B signal is proportional to $\sin \Phi \cos x_N$ as resulting from Eq. (9a) for constant $\sigma(\Phi)$. The ratio of the signals Eqs. (9a) and (9b):

$$\frac{S_A - S_B}{S_A + S_B} = \sin \Phi \cos x_N \qquad (11)$$

becomes independent on material for both the SE and BSE modes. If we assume $k = -1$ for SE which corresponds to a proportionality of the SE yield to $\sec \Phi$ for material with a medium atomic number, then the difference signal becomes:

$$S_A - S_B \propto \tan \Phi \cos x_N = \partial z / \partial x \qquad (12)$$

that is proportional to the gradient $\partial z / \partial x$ of the surface profile $z(x,y)$ where z is parallel to the specimen normal for an untilted specimen. This allows a direct reconstruction of the surface profile on linescans parallel to the x-axis (Fig. 7), that is parallel to the connection of the two detectors, by analogue or digital integration of the difference signal Eq.(12) of two opposite SE detectors (Reimer and Tollkamp 1982, Niemietz and Reimer 1985). The method works for large-scale (Fig.7a) and small-scale structures (Figs. 7b-d). The reconstruction of a step with a height of 2 μm (Fig.7b) shows a tail caused by self-shadowing of the signal for detector B (see discussion below). Such reconstructions have to start with z=0 at x=0 for each line because no information is available about $\partial z / \partial y$. This gradient can be calculated by recording the signals of a pair of SE detectors with a connection line parallel to the y-axis (Niemietz and Reimer 1985). Equations (6) to (10) can be used by substituting
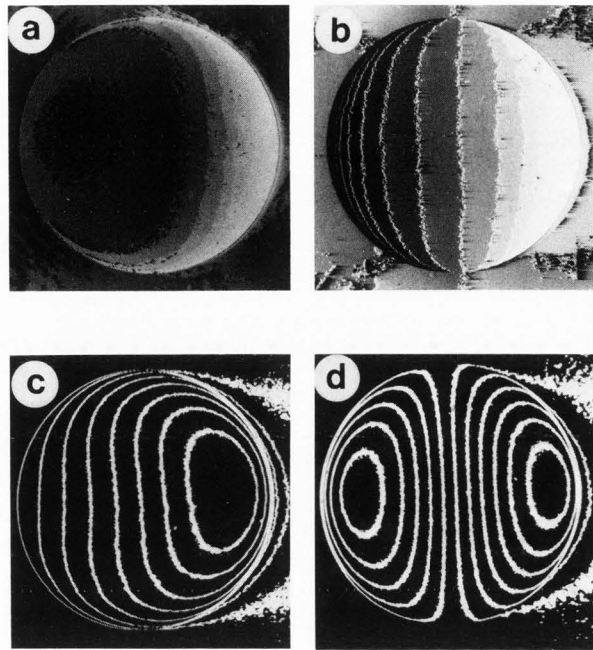

Fig.5. Directly recorded isodensities of a 1 mm steel ball as a test specimen containing all surface inclinations: a) SE A mode, b) SE A-B mode, c) BSE A mode and d) BSE A-B mode.
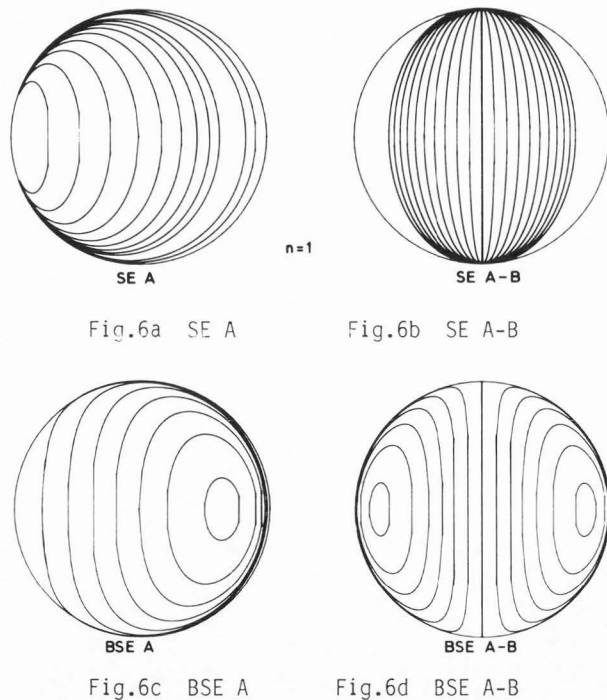

Fig.6a SE A   Fig.6b SE A-B

Fig.6c BSE A   Fig.6d BSE A-B

Fig.6. Calculated isodensities for the four modes a-d shown in Fig.5 assuming $\delta \propto \sec^n \Phi$ and $\sigma_{BSE} \propto \cos^{1/2} \Phi$.
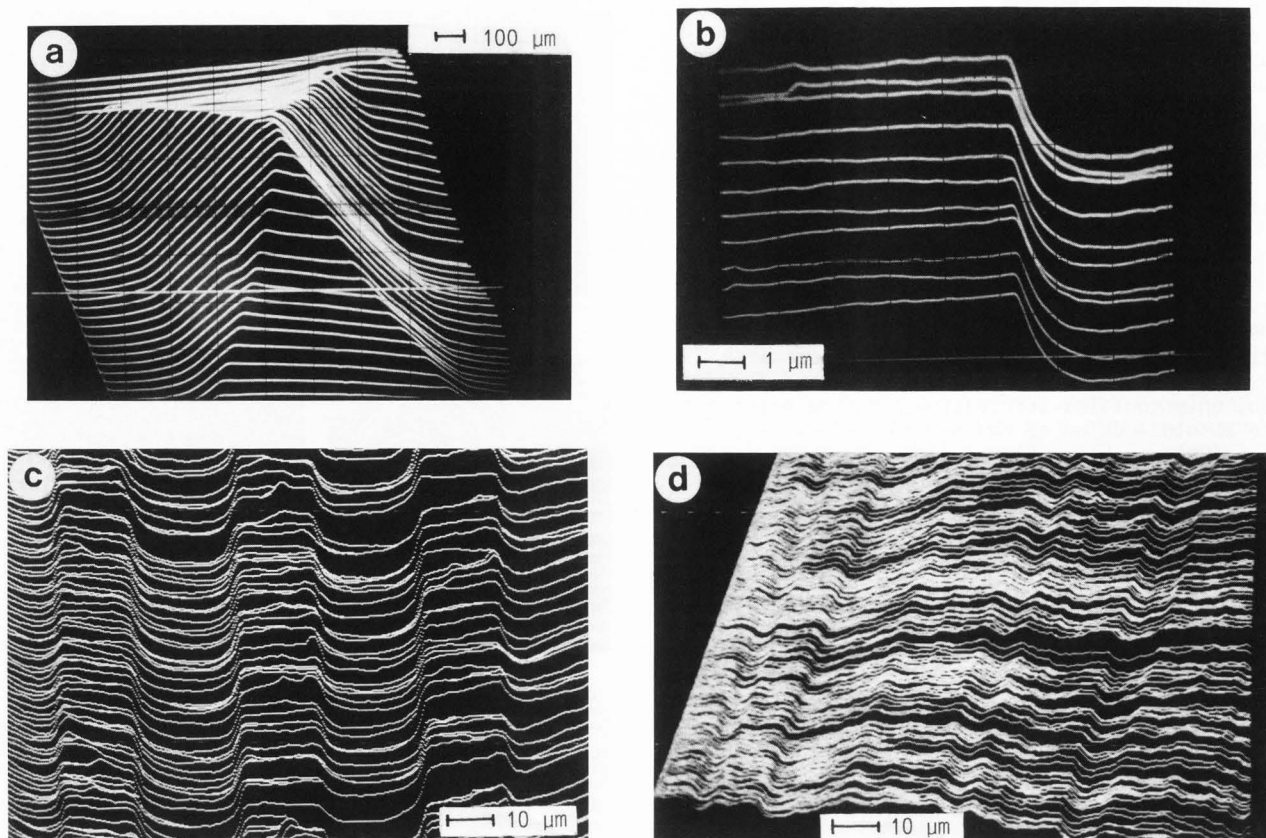
Fig.7.Examples of the reconstruction of surfaces profiles z(x) by analogue or digital integration of the SE A-B signal along single lines for a) a surface replica of a pyramidal indentation (1 x 1 mm), b) a surface step of 2 µm on Al, c) conductive pads on an IC (width: 20 µm, height 2.4 µm) and d) a polished surface (roughness standard).

sin x_N for cos x_N. Equation (11) also holds for a pair of small semiconductor detectors at $\xi=45°$. Using a second pair parallel y, the tilt angle Φ and the azimuthal angle x_N can be calculated and the surface profile can be reconstructed from

$$\partial z/\partial x = \tan \Phi \cos x_N \text{ and } \partial z/\partial y = \tan \Phi \sin x_N (13)$$

(Lebiedzik and White 1975; Lebiedzik et al. 1979; Lebiedzik 1979, Carlsen 1985). Using only $\partial z/\partial x$ from one pair of detectors, distortions in the signal can result in a divergence of parallel profiles as shown in Fig.7d. This can be avoided when using also $\partial z/\partial y$ from another pair of detectors and applying a digital reconstruction technique proposed by Carlsen (1985) for BSE.

It is important for discussing the difference and sum signals of a two-detector system to look also on other types of contrast. The SE A-B image not only increases the topographic contrast and results in an image more analogue to light illumination (Reimer et al. 1984), it also decreases the diffusion contrast (Volbert and Reimer 1980; Reimer 1982; Reimer and Stelter 1987; Reimer et al. 1986) and cancels the material contrast caused

either by differences in atomic number and excited by BSE or by differences in the SE yield and cancels also the channelling contrast of polycrystalline specimens (Volbert and Reimer 1980; Hoffmann and Reimer 1981). The magnetic contrast type 1 increases in the SE A-B mode (Volbert and Reimer 1980; Reimer et al. 1986) and becomes a maximum for a two-detector system because SE deflected by the Lorentz force of external magnetic stray fields towards detector A decrease the signal of detector B and reversely. Therefore, topographic contrast and magnetic contrast type 1 cannot be separated in the difference signal. The SE A+B image shows bright edges independent of their orientation and it becomes difficult to decide whether surface structures are elevations or impressions. A single Everhart-Thornley detector will result in a signal between SE A and SE A+B.

Image irradiance equations for light and electrons in the gradient plane

The image brightness of a surface element depends on its orientation relative to the viewer and to the light source in optics and relative to the electron incidence and to the detector in SEM, respectively. An image irradiance equation has to be developed to relate the geometry and radiometry of image formation. This shall be done in parallel for comparison of the case of light illumination and the SE and BSE modes of SEM. The former parallels that first given by Horn (1977)

but uses notations for the different angles which are used in SEM and are shown in Fig.1 where we made use of the theorem of reciprocity that the viewing direction in SEM corresponds to a direction opposite to the electron incidence and the take-off direction of the detector to a direction opposite to the 'source', respectively:

Φ = surface tilt angle between the beam of primary electrons P and the surface normal N in SEM and

emergent angle between viewer and surface normal in light optics

ξ = take-off angle between detector D and electron beam P in SEM and

incident angle between light source and viewer in light optics

ζ = take-off angle between detector D and surface normal in SEM and

phase angle between light source and surface normal in light optics.

Furthermore, we introduce azimuthal angles x_N and x_D so that the directions of the surface normal and of the detector relative to the electron beam can be described by the pairs Φ, x_N and Φ, x_D, respectively. Such a pair Φ, x_N, for example, corresponds to a point on the unit sphere or can be described by the unit vector:

$$\vec{u} = \begin{bmatrix} \sin \Phi \sin x_N \\ \sin \Phi \cos x_N \\ \cos \Phi \end{bmatrix} = \cos \Phi \begin{bmatrix} \tan \Phi \sin x_N \\ \tan \Phi \cos x_N \\ 1 \end{bmatrix}$$

$$= \cos \Phi \begin{bmatrix} \partial z/\partial x \\ \partial z/\partial y \\ 1 \end{bmatrix} = \cos \Phi \begin{bmatrix} p \\ q \\ 1 \end{bmatrix} \quad (14)$$

in a Cartesian coordinate system where the surface profile can be described by $z(x,y)$. When normalizing the z-component to unity and using Eq. (13), the u- and v-components Eq. (10) become the coordinates:

$$p = \partial z/\partial x = u/(1 - u^2 - v^2)^{1/2}$$
$$q = \partial z/\partial y = v/(1 - u^2 - v^2)^{1/2} \quad (15)$$

of the gradient plane which are directly related to the gradients of the surface element in x and y direction and the surface element can be characterized by the vector $(p,q,1)$ where the z-direction is opposite to the direction of electron incidence. The coordinates u and v of the projection of a sphere are defined inside a unit circle. This projection corresponds to a projection centre at infinity and an equatorial plane as projection plane whereas the projection resulting in the p,q plane has the centre of the sphere as a projection centre and the tangential plane at the north pole as a projection plane. The latter is called a gnomonic projection in crystallography.

The direction of a single distinct light source can be described by the vectors $(p_s, q_s, 1)$ and as shown by Horn (1977) and Woodham (1981), the angles in Fig.1 can be described in the p,q notation by:

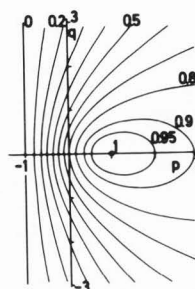$$\cos \Phi = \frac{1}{(1 + p^2 + q^2)^{1/2}} \quad (16a)$$

Fig.8. Isodensities in the p,q plane for a light source at $\xi = 45°$ ($p_s=1$, $q_s=1$) and an observation opposite to the electron beam.

$$\cos \xi = \frac{1}{(1 + p_s^2 + q_s^2)^{1/2}} \quad (16b)$$

$$\cos \zeta = \frac{1 + p\,p_s + q\,q_s}{(1 + p^2 + q^2)^{1/2} (1 + p_s^2 + q_s^2)^{1/2}} \quad (16c)$$

$$\cos x_N = p / (p^2 + q^2)^{1/2} \quad (16d)$$

When assuming a perfectly diffuse surface following Lambert's law, the signal intensity or surface reflectance function for light illumination becomes:

$$S_L = \sigma \cos \zeta \quad (17)$$

The isodensities in the p,q plane are shown in Fig.8 for the light source at $\xi = 45°$ and $x_D=0$ corresponding to $p_s=1$, $q_s=0$ and an observation opposite to the electron beam. The cosine of the phase angle ζ accounts for the foreshortening of the surface element as seen from the source and σ is a reflectance factor. The cosine of ζ can either be calculated by Eq.(16c) or using the notation and the spherical triangle PND of Fig.1:

$$\cos \zeta = \cos \Phi \cos \xi + \sin \Phi \sin \xi \cos(x_D - x_N) \quad (18)$$

When we assume a single distinct detector for BSE and SE for analogy and the validity of Lambert's law Eqs (3) and (5), respectively, the signals of these detectors become:

$$S_{BSE} \propto \eta \cos \zeta \quad (19a)$$

$$S_{SE} \propto \delta(\Phi) \cos \zeta = \delta(0) \sec^n \Phi \cos \zeta \quad (19b)$$

This demonstrates the theorem of reciprocity for light illumination and BSE and SE detection in SEM due to Fig.1, and equations (17) and (19a,b) both become proportional to $\cos \zeta$ though in the case of SE the 'reflectance factor' (SE yield) increases proportional to $\sec^n \Phi$. We discussed above that the BSE signal can decrease in reality proportional to the square root of $\cos \Phi$ for large tilt angles Φ, for example. Consideration of this prefactor by Eq.(16a) results in isodensities for a pair of BSE detectors collecting all BSE with $\xi < \pi/2$ shown in Figs.9a,b for the BSE A and A-B signals. These curves in the p,q plane correspond to Figs. 5c,d in the u,v plane, respectively. This demonstrates that the signal of a single BSE detector A
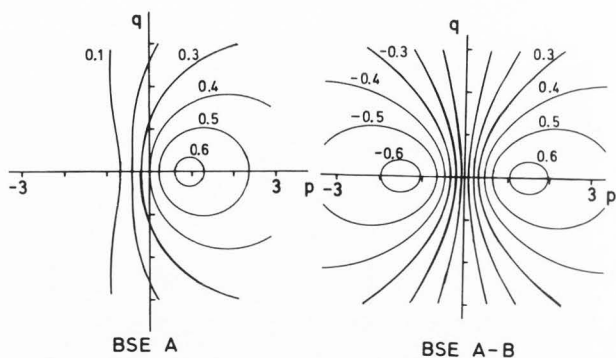
Fig.9. Isodensities in the p,q gradient plane for a single BSE detector A at $(p_s,q_s)=(1,0)$ and for the difference signal A-B of two BSE detectors at $(p_s,q_s)=(\pm1,0)$.
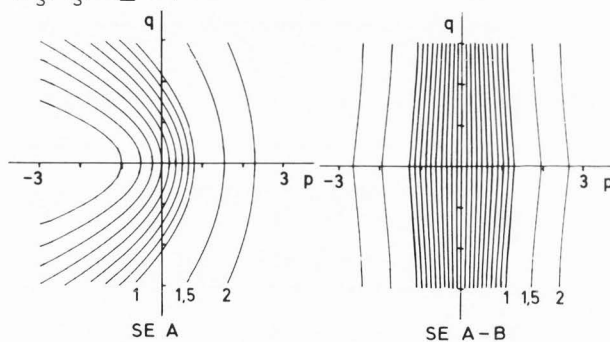

Fig.10a

Fig.10b
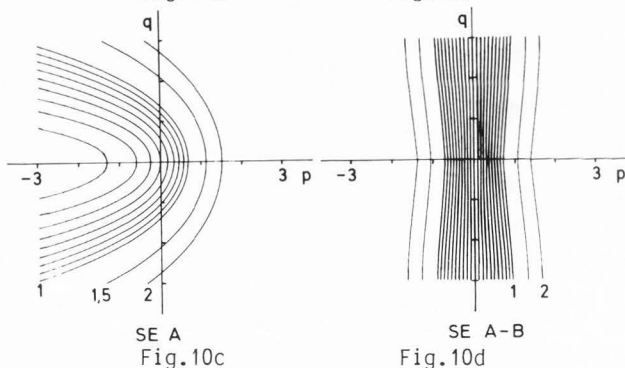

Fig.10c

Fig.10d

Fig.10. Isodensities in the p,q gradient plane for a) and c) the SE signal of detector B and b) and d) the signal A-B of a two-detector system assuming that $\delta \propto \sec^n \Phi$ with n=0.8 (a and b) and n=1.3 (c and d).

in Fig.9a shows isodensities which are similar to those for light illumination under $45°$ in Fig.8.

The isodensities of SE signals in the p,q plane are shown for the case n=0.8 (Figs.10c,d). Figures 10 b and d show the influence of the exponent n of sec Φ on the A-B signal more strongly than the isodensities of single detectors B in Fig.10a and c, respectively. For the case of n=1, analogue to Fig.6b in the u,v plane, the isodensities of the A-B signal in the p,q plane are straight and equidistant lines p=const and the isodensity with the value 1 goes through p=1.

Correction of shadowing and electron diffusion

We showed above that the signal difference of a two-detector system for SE and BSE can be used to calculate the tilt angle Φ and the azimuthal angle x_N of a surface element. The A-B SE signal is directly proportional to $p = \partial z/\partial x$ and a perpendicular detector position results in a signal proportional to $q = \partial z/\partial y$. However, the relations Eqs.(9) and (11) assume a tilted surface without shadowing so that all SE emitted to the left-hand side can be collected by detector A and to the right-hand side by detector B. Figure 4 and equation (7) demonstrate how a surface roughness can limit the sector of emitted SE that are collected by one of the detectors. Such an influence of shadowing and its correction shall be discussed in the following.

We assume a one-dimensional surface profile z(x) for simplicity that is realised in perpendicular scans across IC structures or across surface polishing scratches, for example. This means that the structures show no curvature in y direction (q=0) and the azimuthal angle $x_N = 0$ or π for all surface points. We discussed above how the signals S_A and S_B in Eq.(7) are affected by the shadowing angles $\psi_{A,B}$ and we get:

$$S'_A \propto \sigma(\Phi) \frac{1}{2} (\cos \psi_A + \sin \Phi) \qquad (20a)$$

$$S'_B \propto \sigma(\Phi) \frac{1}{2} (\cos \psi_B - \sin \Phi) \qquad (20b)$$

for $x_N=0$. In the case of secondaries from medium atomic number material with $\sigma(\Phi) \propto \sec \Phi$, the difference signal $S'_A - S'_B$ is not exactly proportional to $\partial z/\partial x$ because of the cos $\psi_{A,B}$ terms and integration of the difference signal results in a first-order surface profile z'(x). From this wrong surface profile z'(x), new shadowing angles ψ'_A and ψ'_B can be calculated and we get a correction $\Delta S_{A,B}$ of the original signals S'_A and S'_B by adding for each image point that sectors of the exit characteristics which are shadowed:

$$S'_{A,B} = \sigma(\Phi) \frac{1}{2} (1 - \cos \psi'_{A,B}) \qquad (21)$$

Integration of $S'_A - S'_B + k (\Delta S'_A - \Delta S'_B)$ results in a corrected profile z''(x) which results in new corrections $\Delta S''_{A,B}$ at the original signals S'_A and S'_B.

Figures 11 show the result of such an iteration for a bar and a groove. The line profiles z'(x) in first-order approximation have been obtained by integration of calculated S'_A and S'_B signals. Shadowing results in a long tail in front of and behind the bar and a decrease of surface elevation and depression for bars and grooves, respectively. In case of the bar, two or three iteration steps are sufficient to reconstruct the true profile. However, it becomes difficult to get the correct profile of a groove with a small number of iteration steps.

This shows that a correction scheme for compensating the influence of shadowing is possible. However, this method only works for structures large compared to the electron range R. Figure 12 shows the dependence of R on electron energy E
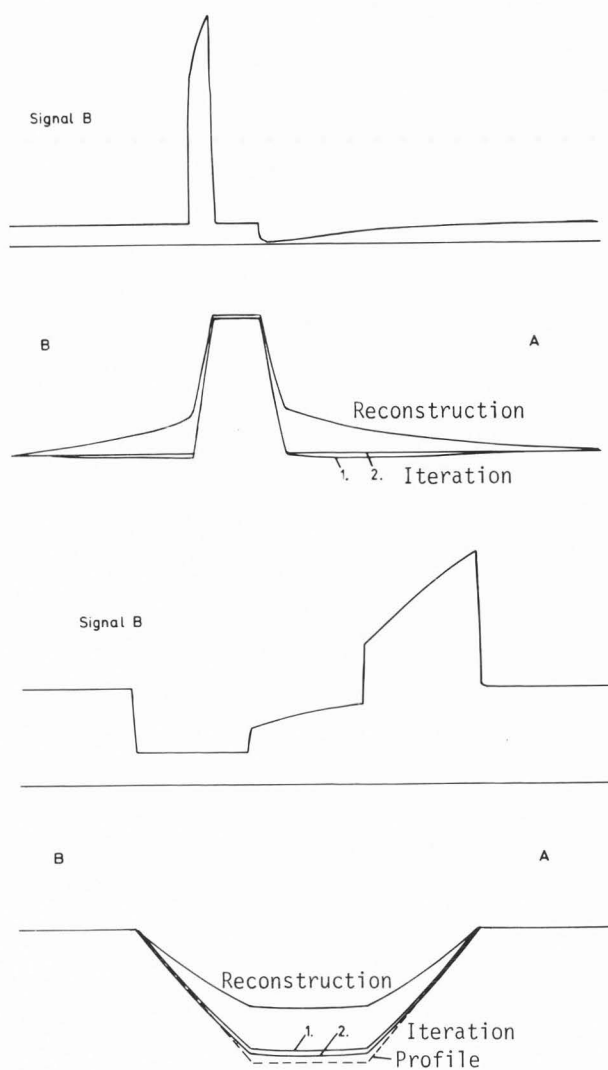
Fig.11. Model calculation for demonstrating the iteration scheme to correct shadowing of the specimen for a bar and a groove.

Fig.12. Double-logarithmic plot of electron range R versus electron energy E using equation (22) and measurements of Al-Ahmad and Watt (1983).

using the estimation

$$R = \frac{20}{3} E^{5/3} \qquad (22)$$

with R in $\mu g\ cm^{-2}$ and E in keV. This formula assumes that the range in units of mass-thickness is independent of atomic number. Figure 12 also contains experimental values of R measured by Al-Ahmad and Watt (1983) which depend on the extrapolation method applied to transmission experiments on thin films. Transmission curves of films of high atomic number show a longer tail than those of low atomic number material. The comparison of these experiments with the simple formula (22) show that this formula can be used down to E = 1 keV for estimating the range.

When the structure, e.g., the height of a surface step, becomes comparable or smaller than R, electron diffusion effects have to be taken into account. (The complexity of the signals S_A

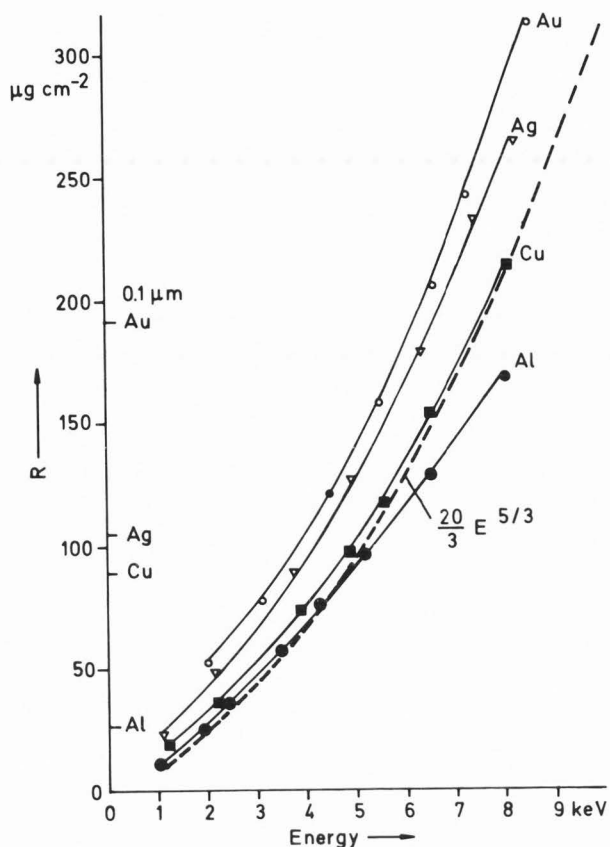and S_B is demonstrated in Monte Carlo calculations by Reimer and Stelter (1987).). The effect of electron diffusion resulting in wrong surface profiles can be reduced when decreasing the primary electron energy. Figure 12 shows that R approaches the exit depth $t \simeq$ 2-5 nm of SE and/or the resolution (2-10 nm) of a SEM for E < 1 keV.

References

Al-Ahmad KO, Watt DE (1983) Stopping power and extrapolated ranges for electrons (1-10 keV) in metals. Phys.Rev. 16, 2257-2267.

Carlsen IC (1985) Reconstruction of true surface-topographies in SEM using backscattered electrons. Scanning 7, 169-177.

Castaing R (1960) Electron probe microanalysis. Adv.Electr.Electr.Phys. 13, 317-386.

Darlington EH (1975) Backscattering of 10-100 keV electrons from thick targets. J.Phys. D8, 85-93.

Drescher H, Reimer L, Seidel H (1970) Rückstreukoeffizient und Sekundärelektronenausbeute von 10-100 keV Elektronen und Beziehungen zur Rasterelektronenmikroskopie. Z.angew.Phys. 29, 331-336.

Everhart TE, Thornley RFM (1960) Wideband detector for micro microampere low-energy currents. J.Sci.Instr. 37, 246-248.

Herrmann R, Reimer L (1984) Backscattering

coefficient of multicomponent specimens. Scanning 6, 20-29.

Hoffmann M, Reimer L (1981) Channelling contrast on metal surfaces after ion beam etching. Scanning 4, 91-93.

Horn BKP (1977) Understanding image intensities. Artificial Intelligence 8, 201-231.

Horn BKP, Brooks MJ (1986) The variational approach to shape from shading. Computer Vision, Graphics and Image processing 33, 174-208.

Ikeuchi K, Horn BKP (1981) Numerical shape from shading and occluding boundaries. Artificial Intelligence 17, 141-184.

Jackman J (1980) New scanning electron microscope depends on multi-function detector. Industrial Res. and Develop., ISSN 0160-4074, Eindhoven, Netherlands.

Kanter H (1957) Zur Rückstreuung von Elektronen im Energiebereich von 10-100 keV. Ann. Phys. 20, 144-166.

Kimoto S, Hashimoto H, Suganama T (1966) Stereoscopic observation in scanning microscopy using multiple detectors. In: The Electron Microprobe, (eds) McKinley TD et al., John Wiley and Sons, New York 480-498.

Lange M, Reimer L, Tollkamp C (1984) Testing of detector strategies in SEM by isodensities. J.Microsc. 134, 1-12.

Lebiedzik J (1979) An automatic surface reconstruction in the SEM. Scanning 2, 230-237.

Lebiedzik J, White EW (1975) Multiple detector method for quantitative determination of microtopography in the SEM. Scanning Electron Microsc. 1975: 181-188.

Lebiedzik J, Lebiedzik J, Edwards R, Phillips B (1979) Use of microtopography capability in the SEM for analysing fracture surface. Scanning Electron Microsc. 1979; II: 60-66.

Lödding B, Reimer L (1981) Monte-Carlo-Rechnungen im Energiebereich 1-20 keV. Beitr. elektr. mikr. Direktabb. Oberfl. 14, 315-324, Remy Münster.

Moll SH, Healey F, Sullivan B, Johnson W (1979) A high efficiency, non-directional backscattered electron detection mode for SEM. Scanning Electron Microsc. 1979; II:303-310.

Niedrig H (1982) Electron backscattering from thin films. J.Appl.Phys. 53, R15-R49.

Niemietz A, L. Reimer (1985) Digital image processing of multiple detector signals in SEM. Ultramicroscopy 16, 161-174.

Reimer L (1982) Electron signal and detector strategy. In: Electron Beam Interactions with Solids, (eds.) Kyser DF et al., SEM Inc., AMF O'Hare, Chicago IL 60666, 299-310.

Reimer L (1984) Quantitative SEM of surfaces. J. de Physique 45, colloque C2, 291-296.

Reimer L (1985) Scanning Electron Microscopy, Physics of Image Formation and Microanalysis, Springer, Berlin, Heidelberg New York, Tokyo.

Reimer L, Drescher H (1977) Secondary electron emission of 10-100 keV electrons from transparent films of Al and Au. J.Phys. D10, 805-815.

Reimer L, Riepenhausen M (1984) Dependence of the signal of backscattered electrons on surface tilt and take-off angles. Eighth Europ. Congr. Electr.Micr. Vol.1, 641-642, Congr.Bureau MOTESZ, Budapest, Hungary.

Reimer L, Riepenhausen M (1985) Detector strategy using multiple detector systems. Scanning 7, 221-238.

Reimer L, Stelter D (1986) Fortran 77 Monte Carlo program for minicomputers using Mott cross-sections. Scanning 8, 257-277.

Reimer L, Stelter D (1987) Monte Carlo calculation of electron emission at surface edges. Scanning Microsc. 1 (3), 951-962.

Reimer L, Tollkamp C (1980) Measuring the backscattering coefficient and secondary electron yield inside a SEM. Scanning 3, 35-39.

Reimer L, Tollkamp C (1982) Recording of topography by secondary electrons with a two-detector system. Electron Microscopy 1982, Vol.2 593-594. Deutsche Ges. für Elektronenmikr., Frankfurt

Reimer L, Volbert B (1979) Detector system for backscattered electrons by conversion to secondary electrons. Scanning 2, 238-248.

Reimer L, Volbert B (1980a) New detector system for conversion of backscattered to secondary electrons. Inst. Phys. Conf. Ser. No. 52, 89-92, London.

Reimer L, Volbert B (1980b) Separation of topographic and material contrast in SEM by different detector systems. Electron Microscopy 1986, 3, 172-173, Seventh Europ. Congr. Electr. Microsc. Found., Leiden, Netherlands.

Reimer L, Volbert B (1982) The origin and correction of SEM image artifacts arising from the use of the difference signal of the two detectors. Philips Electron Optics. Bull. No. 118.

Reimer L, Riepenhausen M, Tollkamp C. (1984) Detector strategy for improvement of image conrast analogous to light illumination. Scanning 6, 155-167.

Reimer L, Riepenhausen M, Schierjott M (1986) Signal of backscattered electrons at edges and surface steps. Scanning 8, 164-175.

Volbert B, Reimer L (1980) Advantages of two opposite Everhart-Thornley detectors in SEM. Scanning Electron Microsc. 1980; IV:1-10.

Wells OC (1974) Scanning Electron Microscopy MacGraw-Hill, New York.

Woodham RJ (1981) Analysing images of curved surfaces. Artificial Intelligence 17, 117-140.

Discussion with Reviewers

DC Joy: How would sample charging effect this computation ? Could the correct result be obtained iteratively, as is the case for shadowing, or must some other method be employed?
Authors: For example, we observed that positively charged dust particles produce an artificial surface structure in the SE A-B image. No effect is observed in the BSE A-B image. Therefore, comparison of SE and BSE records can separate charging from topographic contrast.

DC Joy: Could still better, or more robust, results be achieved by using more than two detectors ?
Authors: Yes, by a four-detector system recording SE or BSE.

DC Joy: Is it necessary to take special precautions to ensure that the response of your detectors and amplifiers remain linear and stable when applying this technique ?
Authors: Yes, but a large problem is the local variation of image intensity. Very important is the recording of the zero signal level for digital image processing of this type.

MG Rosenfield: Have you compared your reconstructed, simulated images to SEM cross-sections to see how good the agreement is between theory and experiment ?
Authors: No, but stereoscopy and cross-sections shall be used in future for comparison.

MG Rosenfield: Do you think this technique will work at the low 1 kV range voltages used to inspect IC wafers? If so, could this work be applied to low voltage linewidth measurement of uncoated resist features? Have you investigated this?
Authors: Because of the strong decrease of the electron range, diffusion contrast can be suppressed at electron energies of 1 keV and the signal more depends on surface topography. For a measurement of linewidth one should keep in mind what width is wanted, at the top or bottom, for example. Monte Carlo calculations can help to calculate the detector signals and look on special features of the linescan which can be measured with high accuracy. We observed qualitatively the influence of low voltage on the SE A-B images of conductive pads on ICs (Reimer et al. 1986).

H Niedrig: What are the objects in Figs. 8 to 10?
Authors: These diagrams show isodensities in the gradient plane and the advantage of such diagrams is just that the plot becomes independent of specimen structure.

H Niedrig: Fig.11: How do the signals A look like? (Presumably symmetric to a central vertical mirror plane?)
Authors: Yes.

Z. Radzimski: The number of assumptions in the proposed method limit the surface reconstruction to only a smooth relief on homogeneous material. Is it possible to introduce various "correction" terms that deal with edges, points, extreme angles, etc. which are not strictly integrable?
Authors: This is just the future aim of our work, to use a data base in a computer which takes into account the electron-specimen interactions.

Z Radzimski: Would you explain in detail the range of applications for which the shadowing methods compete with stereoscopy, which seems to be a proven technique for accurate surface reconstruction?
Authors: Stereoscopy is indeed a very accurate method due to the capability of the human vision system to detect very small parallaxes. Stereoscopy can be transferred to digital image processing by searching the maximum of correlation when a window of the second micrograph is shifted across a reference window in the first micrograph.

Because of noise this method can result in errors. The future aim will be to combine the method of shape from shading which needs no sharply image points with the digital stereoscopy. The latter can calculate the specimen height at image points showing a good correlation and the image is "filled" by the shape from shading method.

Z Radzimski: Can you discuss the advantages and disadvantages of using high energy backscattered electrons for accurate measurements of surface topography?
Authors: The method fails especially when the specimen structure is of the order of the electron range. The influence of the diffusion contrast which causes the largest trouble to be compensated can be suppressed either by using very low voltages or very high voltages so that the range is larger than the structure. In the latter case a diffuse background caused by diffusion has to be subtracted.

BKP Horn: What happens when the reflectance map does not consist exactly of parallel straight lines (k=-1)? How is the accuracy affected? How can modern SFS methods be used to deal with this case? How can neighbouring contours be "tied together to obtain a surface?
Authors: When the isodensities are not straight lines wrong surface tilts result. When applying the method in future, isodensities can be recorded on a small steel ball as specimen and the stored data can be used for a more correct determination of surface tilt. The best way to tie-together contours will be to use an additional pair of detectors in the perpendicular direction or to apply stereoscopy on a distinct number of image points.